Volume 16, Issue 3, 162523 (1-12)

International Journal of Nano Dimension (IJND)

https://dx.doi.org/10.57647/j.ijnd.2025.1603.23

Effects of chirality and functionalization of carbon nanotubes as nanocarriers on the adsorption of Lenalidomide anticancer drug: Insights from molecular dynamics simulation

Hamidreza Dehghan[1], Yadollah Saghapour[1], Arezoo Tahan[2,*], Shiva Joohari[3], Arezoo Ghadi[4]

[1]*Department of Chemistry, Gachsaran Branch, Islamic Azad University, Gachsaran, Iran.*
[2]*Department of Chemistry, Semnan Branch, Islamic Azad University, Semnan, Iran.*
[3]*Department of Chemistry, Yasouj Branch, Islamic Azad University, Yasouj, Iran.*
[4]*Department of Chemical Engineering, Ayatollah Amoli Branch, Islamic Azad University, Amol, Iran.*

[*]**Corresponding author:** arezoo.tahan@gmail.com

Original Research

Received:
1 November 2024
Revised:
24 January 2025
Accepted:
6 February 2025
Published online:
1 June 2025

Abstract:

In this study, the adsorption process of Lenalidomide (LEN) anticancer drug on carbon nanotubes (CNTs) with different chiralities was studied using molecular dynamics (MD) simulations. Chirality effects of CNTs (zigzag (10,0), chiral (10,5) and armchair (10,10)), their functionalization with carboxylic functional groups and solubility were investigated. Results showed that the interaction strength of LEN/water molecules with CNTs and f-CNTs (carbon nanotubes functionalized with carboxylic functional groups) was as a function of chirality. LEN molecules were considerably adsorbed on the f-CNT surface with (10,10) chirality which was recognized via the most negative van der Waals (vdW) energy and the greatest number of atomic contacts (nAC). Moreover, the number of hydrogen bonds (nHBs) between f-CNT (10,10) and solvent molecules was higher than for the other f-CNTs. The highest value of solvent accessible surface area (SASA) 45 nm^2 for the f-CNT (10,10) compared with the other CNTs confirmed that armchair f-CNT had larger surface area accessible for interacting with the solvent. The functionalization of CNTs led to a decrease in solvation free energy (ΔG_{sol}) and an increase in SASA which resulted in better solubility of f-CNTs in water. Based on the finding, f-CNTs were proposed highly efficient candidate for drug delivery.

Keywords: Carbon nanotubes; Chirality; Drug delivery; Lenalidomide drug; Molecular dynamic simulation

1. Introduction

Lenalidomide (LEN) under the brand name Revlimid, a thalidomide analogue, is an immunomodulatory agent with antiangiogenic and antineoplastic properties. The chemical name is 3-(4-amino-1-oxo 1, 3- dihydro-2H-isoindol-2-yl) piperidine-2,6-dione. The Lenalidomide (LEN) drug chemical structure and characteristics is presented in (figure 1, and Table 1). It's widely used to treat various cancers such as multiple myeloma (MM), chronic lymphocytic leukaemia (CLL), prostate cancer, renal cancer, pancreatic cancer, myelodysplastic syndromes (MDS) and advanced ovarian cancer [1, 2]. MM is a form of blood cancer, specified by the accumulation of a plasma cell clone in the bone marrow. Traditional therapies for treatment of MM were based on cytotoxic or antiproliferative agents such as mephelan and doxorubicin [3]. More specifically targeted therapies such as imatinib (ABL), the small-molecule inhibitors, and monoclonal antibodies, rituximab (CD20), and alemtuzumab (CD52) are also available for MM. However, all of the agents have single modes of action, which although effective, target few of the pathways that are involved in these diseases [4]. The requirement for multi-modal therapy in these diseases has resulted in the trial of agents such as thalidomide and its analogues such as lenalidomide, which are anti-metastatic, anti-angiogenic and also augment anti-tumor immunity [5]. LEN can cause significant neutropenia

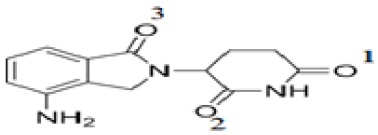

Figure 1. The chemical structure of Lenalidomide (LEN) drug.

and thrombocytopenia [6]. LEN has indicated significant improvement in overall survival for myeloma (that generally carries a low prognosis), however toxicity remains a problem for patients [7]. Due to its low solubility in water, LEN has low oral bioavailability (below 33%), and as a direct result of this, the frequency of dosing increases, thereby increasing the risk of toxicity. Also, low efficiency, poor membrane permeability, short in-vivo half-life ($3-4$ h), and severe side effects like anemia or leukopenia have led to research on its nano delivery approach. Besides, only 20% of the oral dose is effective, and the rest is rapidly excreted via urine, which explains the need to adjust its dose, which has a higher risk of side effects in the renal system [8]. Therefore, a controlled drug delivery to the tumor microenvironment could mitigate these issues.

Nowadays, drug delivery has been used as a new method to directly send anticancer drugs to target tissues for reducing the side effects of drug toxicity. Controlling the rate and/or the location of drug release, facilitating drug absorption and increasing drug efficiency are the main concerns in utilization of drug delivery systems (DDSs) [9]. Recently, molecular dynamics (MD) simulations, and density functional theory (DFT) method compute a wide variety of properties of almost any kind of atomic system: molecules, crystals, and surfaces, the field of medicine has benefited a lot from this technology [10–12], and one of its popular examples is the introduction of various types of nanoparticles as drug delivery systems and drug release systems in general [13, 14]. By precisely delivering medication to specific targets at predetermined times, this new system offers superior efficacy and safety compared to traditional, systemic drug administration [15].

Nano-carriers have been extensively studied over the past decades and are designed to improve clinical efficiency while reducing the toxicity associated with traditional intravenous administration methods. Moreover, they have shown promising results in drug delivery [16–18]. Nanotube-based drug delivery systems have received considerable attention due to their salient features, such as high surface area to volume ratio for encapsulating different drugs and their ability to penetrate into cells, tissues and bacteria due to their open ends. Therefore, it is important to understand drug-nanotube interactions in order to evaluate drug encapsulation behavior in nanotubes [19–22]. Drug encapsulation inside the nanostructure is challenging because not only does it need to carry the drug without any chemical modification, but also it is necessary for releasing the drug near the cancer cells. Various nano-carriers have been approached for targeted delivery of LEN in cancer therapy with promising results over the past few decades, including Gold, Lactoferrin, PLGA (Poly-lactic-co-glycolic acid) and chitosan nanoparticles as a carrier for the LEN delivery [23–26]. The investigated β-cyclodextrin oligosaccharides as nanocarrier for LEN anticancer [27]. Also, the conducted density functional theory (DFT) and TD- DFT calculations to understand the adsorption mechanism of LEN anticancer on $B_{12}N_{12}$ nanocluster surface [28]. The results revealed that the LEN adsorption from the O1 on the $B_{12}N_{12}$ nanocluster leads to higher electrical conductivity than the other active sites. The results revealed that the LEN adsorption from the oxygen atom on the $B_{12}N_{12}$ nanocluster leads to higher electrical conductivity than the other active sites. They showed that the interactions are mostly non-covalent in nature. Their findings indicated that the $B_{12}N_{12}$ could serve as a suitable biomedical carrier for delivering the LEN drug.

Numerous theoretical have explored the interactions between anticancer drugs and the CNTs and f-CNTs using MD simulations and DFT calculations [29–33]. As can be seen, most of the studies conducted in the field of LEN drug delivery have been done with DFT methods. Thus the present study investigates the interaction of LEN molecules with the CNTs and f-CNTs using MD simulation. It is proved that one of the most effective carriers for DDS are carbon nanotubes (CNTs) [34]. CNTs possess a remarkable ability to transport molecules across cell membranes due to their very high specific surface area [35, 36]. However, the CNTs are chemically neutral in nature and insoluble in water. Covalent or noncovalent functionalization is performed to dissolve them in water. These corrections may change the CNT nature, such as the solubility, reducing toxicity and tumor retention [37, 38]. According to the studies, no simulation has been done with these structures are CNTs and f-CNTs.

In this research, we conducted a detailed investigation and comparison of the adsorption behavior of the LEN drug on the surface of both CNTs and f-CNTs. The MD simulations were performed to study the effects of chirality and carboxylic functional groups on the vdW interactions and HBs between LEN molecules and the CNT/f-CNTs. Furthermore, we completely studied the influence of carboxylic functional groups and chirality on solubility of CNTs in solvent. The main aim of this work was to propose a suit-

Table 1. Characteristics of Lenalidomide (LEN) drug.

Drug	Lenalidomide (LEN)
Chemical formula	$C_{13}H_{13}N_3O_3$
Molecular weight	259.265 (g mol^{-1})
IUPAC name	3-(4-Amino-1-oxo-1,3-dihydro-2*H*-isoindol-2-(3RS-yl) piperidine-2,6-dione)
Floor	Anticancer

able DDS for LEN that has good solubility in water, thereby improving LEN bioavailability and reducing its toxicity.

2. Experimentals

2.1 Simulation details

In this paper, the MD simulations were used to study the effects of chirality and carboxylic functional groups on the interaction of LEN drugs with both CNTs and f-CNTs. Details of the simulated systems were shown in (Table 2, and Fig. 2). Three kinds (zigzag (10,0), chiral (10,5) and armchair (10,10)) of CNTs, which were built using the Charmm-gui (50) online server were chosen [39]. For constructing f-CNTs, 24 carboxyl functional groups were randomly attached to both ends and walls of CNTs (4 carboxyl functional groups were placed at each end of the nanotubes and 16 carboxyl groups were placed on the surface of the nanotubes). The MD simulations were conducted applying Gromacs software [40], with CHARMM36 force field [41]. The calculations were performed using a 32-core virtual processor and 64GB of RAM under the Linux operating system. In each simulation system, one nanotube molecule (CNT or f-CNT) and five drug molecules were randomly placed inside a cubic box with dimensions $6 \times 6 \times 6$ nm subjected to periodic boundary conditions in all dimensions. The studied systems were completely hydrated by solvent molecules utilizing the single point-charge TIP3P model [42]. In drug adsorption onto the CNTs and f-CNTs, all heavy atoms of the f-CNTs/CNTs were fixed at their position by applying an imaginary spring with a force constant of 1000 kJ.Mol^{-1}.Nm^{-2} where the functional groups were allowed to relax but the water molecules could move freely in the simulation box. To keep the bonds between hydrogen and heavy atoms at their equilibrium length, the LINCS algorithm was used. For calculating long-range electrostatic interactions, Particle-Mesh- Ewald (PME) method was applied [43]. The grid algorithm was used to search for neighboring grid cells during the PME calculations. After ensuring that the simulation cells had achieved equilibration, by energy minimization using steepest descent algorithm, the temperature was kept constant (310 K) in the NVT ensemble for 20 ns and then pressure (1 bar) and density were kept constant in the NPT ensemble for 20 ns. Finally, the simulations were carried out at a constant temperature of 310 K and a pressure of 1 bar using the Berendsen barostat method [44]. The time step for the simulation was set at 2 fs. The simulation systems were neutral, meaning they had a net charge of zero and their dynamics was simulated for 50 ns.

3. Results and discussion

3.1 Equilibrium state

In this research, the stability of simulation systems was studied using root- mean- square deviation (RMSD) curves: (10,0), (10,5) and (10,10) CNTs and f-CNTs with five LEN drug molecules in the solvent [43, 44]. RMSD represents the mean displacement of a molecule during the simulation time relative to the reference structure at the start of the simulation. The findings showed that all systems attained an equilibrium state after 1ns, as shown in Fig. 3.

Table 2. Details of the simulated systems.

	Name	# of atoms	Diameter (nm)	Length (nm)
CNT	(10,0)	360	~ 0.765	~ 3.57
	(10,5)	440	~ 1.032	~ 3.355
	(10,10)	600	~ 1.37	~ 3.52
f-CNT	(10,0)	448	~ 0.765	~ 3.75
	(10,5)	538	~ 1.032	~ 3.355
	(10,10)	688	~ 1.37	~ 3.52

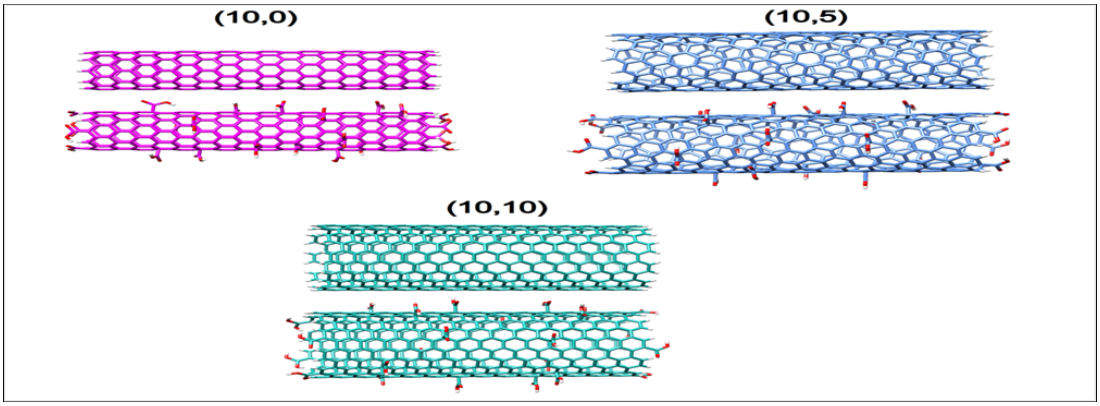

Figure 2. Functionalized nanotubes with carboxyl functional groups (f-CNTs), and CNTs with different chirality used in this study.

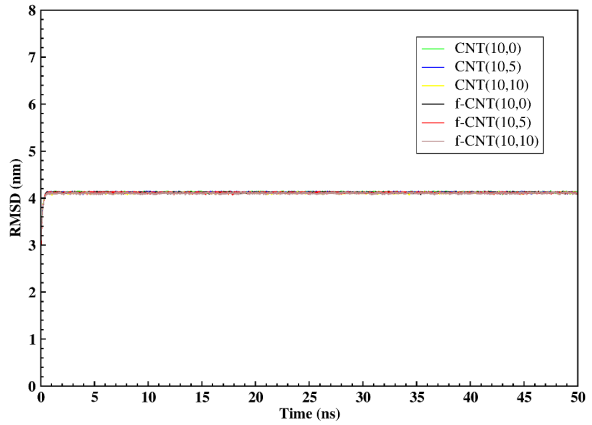

Figure 3. RMSD curves of LEN/f-CNTs and LEN/CNTs systems with different chiralities as a function of the simulation time.

3.2 Radius of gyration (Rg)

One of the suitable parameters to investigate the rate of accumulation of ligand molecules is to check the changes in the Rg of the drug molecules during the simulation time. As we know, Rg reduction indicated more accumulation of ligand molecules in one area. A higher Rg implied higher dispersion of the molecules. In this study, the decrease in the Rg values in the shortest time from the molecular dynamics simulations indicated the high rate of drug accumulation around f-CNTs/CNTs. The Rg plots in Fig. 4 showed drug molecules accumulated around the CNTs after about 3 ns, and the Rg values reached about 2 nm in each simulation. While, in the presence of f-CNTs, the Rg values reached about 2.6 nm in the same time (3 ns). As can be seen from the Figs. 4 (a, b), the Rg values in the presence of all CNTs, especially CNTs (10,10) and (10,0) (Fig. 4 (a)), and in the presence of f-CNTs (10,10) and (10,5) (Fig. 4 (b)), had a considerable decreasing trend at the most simulation times and at the end of the simulation, it reached an approximate value of 1nm, which indicated more accumulation of drug molecules around the mentioned f-CNTs/CNTs. In addition, Rg fluctuations were more intense in presence of f-CNTs than CNTs. The possible reason for high fluctuations of Rg in f-CNTs could be the presence of carboxyl functional groups on the nanotube surfaces, as a result of which the drug molecules could not fully interact with the nanotube surfaces and a part of the drug molecules was free.

3.3 Radial distribution functions (RDF)

The RDF analysis provided valuable insights into the adsorption process of LEN on the surfaces of f-CNT and CNT in water. The RDF plots in Figs. 5 (a, b) showed sharp peaks that exhibited strong interactions between LEN and f-CNTs/CNTs. Based on the findings, the main interactions between LEN molecules and f-CNTs/CNTs were observed at distance ranging approximately $0.5 - 1.9$ nm, and the highest level of interactions between the adsorbed drugs and the nanotube surfaces were at 0.6 nm. It was found that the strength of the RDF profile between the CNTs and LEN (Fig. 5 (a)) molecules was higher than the RDF magnitude in the f-CNTs (Fig. 5 (b)) and the functionalization of CNTs has only increased RDF value in armchair nanotube (10,10) [45, 46]. The sharp peaks in CNTs were likely a result of $\pi - \pi$ stacking (pi-stacking) interactions between aromatic rings of LEN molecules and the sidewalls of CNTs and also the formation of a few Pi-donor interactions between amidic groups of LEN and CNT sidewalls (Fig. 6). In this regard, carboxylic functional groups in f-CNTs could be considered as a barrier to establish pi-stacking interactions between the nanotube and the drug.

Additionally, the most intense peaks were observed in the CNT (10,0) and f-CNT (10,10) systems which showed that these systems had more interactions with LEN than the other ones. The probable reason of high RDF value for f-CNT (10,10) might be penetration of two drug molecules into the nanotube and the participation of both internal and external sidewalls of f-CNT in pi-stacking interactions with the drug molecules (Fig. 7) [47, 48].

To comprehend the molecular orientation of LEN adsorbed on CNT (10, 0) and f-CNT (10, 10) with the most intense

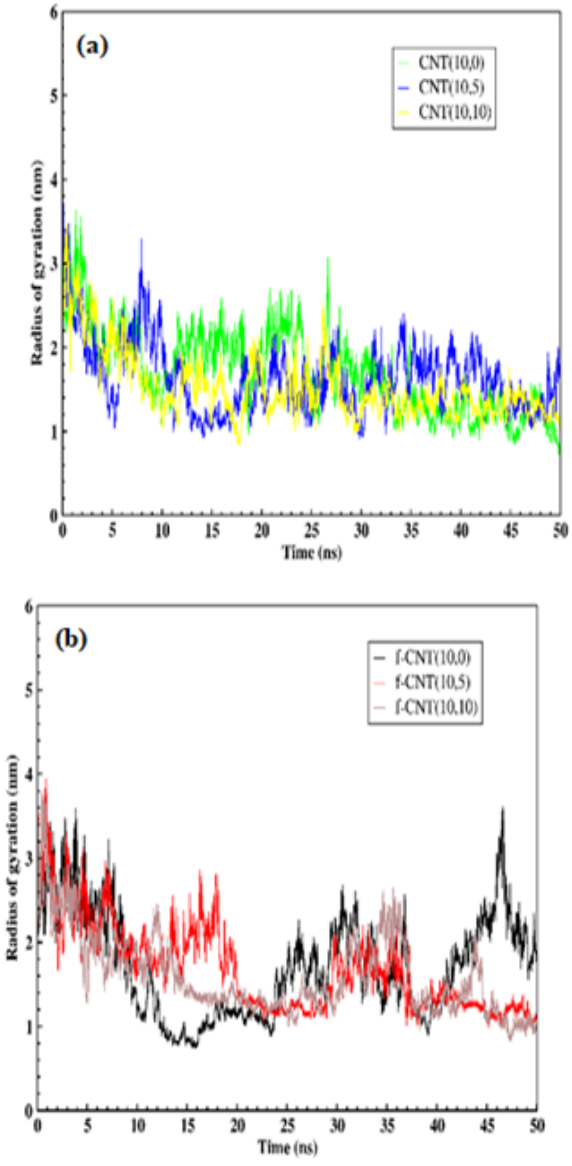

Figure 4. Radius of Gyration of LEN drug molecules around CNTs (a) and, f-CNTs (b) with different chiralities in the simulation systems.

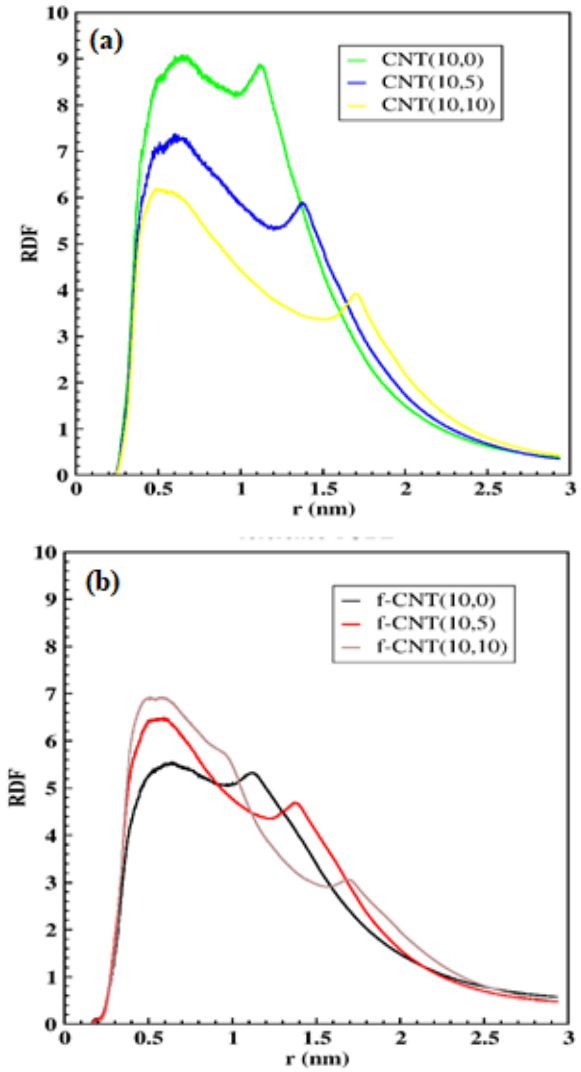

Figure 5. RDF of LEN drug molecules around CNTs (a) and f-CNTs (b) with different chiralities in the simulation systems.

RDF peaks and role of LEN (Fig. 8 (a)) different parts in the interaction with the surfaces of the mentioned nanotubes, the atomic RDF diagram was used. For this reason, the LEN molecule was divided into two parts and two atoms from each part were chosen as representatives of each Part (C_2 and N_2 as representatives of part 1 and N_3 and C_{11} as representatives of Part 2) (Figs. 8 (a, b, c)). It was observed that the sharp peaks for atomic representatives of aromatic rings in CNT (10,0) were located at $0.5 - 1.2$ nm, while the sharp peaks for atomic representatives in f-CNT (10,10) were located between 0.40 and 1.7 nm (Figs. 8 (b, c)). In addition, the RDF values between the f-CNT/CNT and atomic representatives of part 1 were significantly higher than the RDF magnitude of atomic representatives of part 2. These results showed that LEN molecules interacted with the f-CNT/CNT surface from the side of part 1 and adsorbed on their surfaces.

3.4 The van der Waals energy

The energy values of vdW interactions between the LEN molecules and both CNTs and f-CNTs were computed and presented in Figs. 9 (a, b). As all the partial charges of the atoms in LEN molecules and the f-CNTs/CNTs have been set to zero, the electrostatic interactions did not participate in the overall interaction energy. Consequently, the MD descriptions of the interactions between f-CNTs/CNTs and LEN molecules were determined solely by vdW interactions and HBs. The curves illustrated that functionalization of CNTs increased vdW interactions in armchair and chiral nanotubes [38, 47, 48]. The strength of interaction between LEN molecules and f-CNTs/CNTs depended on the nanotube chirality. The trend of the vdW interactions between LEN molecules and f-CNTs and CNTs was similar and it followed the order of (10,10) > (10,5) > (10,0) at the corresponding simulation systems. But, their fluctuations were more intense in f-CNTs than CNTs. Fig. 9 (b) showed that in the CNT/f-CNT (10,0), the vdW interactions were weaker than other systems, and at 32 ns and 47 ns of simulation time, the vdW energy values for f-CNT (10,0) were close to zero. The reason for this observations could be desorption of two drug molecules from the f-CNT (10,0) surface (Fig. 10) at the mentioned times. Furthermore, the highest vdW interactions between drug molecules and f-CNT (10,0) were

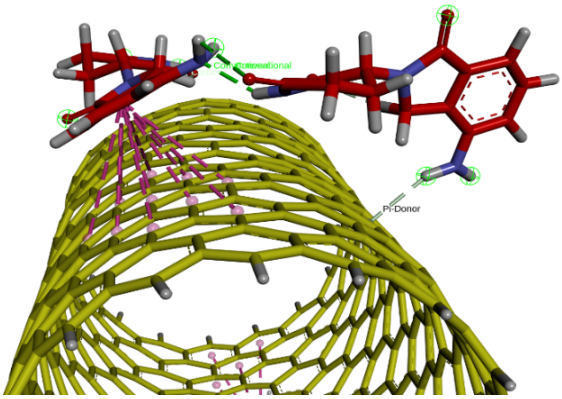

Figure 6. The pi-stacking interactions between aromatic rings of LEN molecules and CNT sidewalls along with Pi-donor interactions between amine groups of LEN molecules and CNT sidewalls.

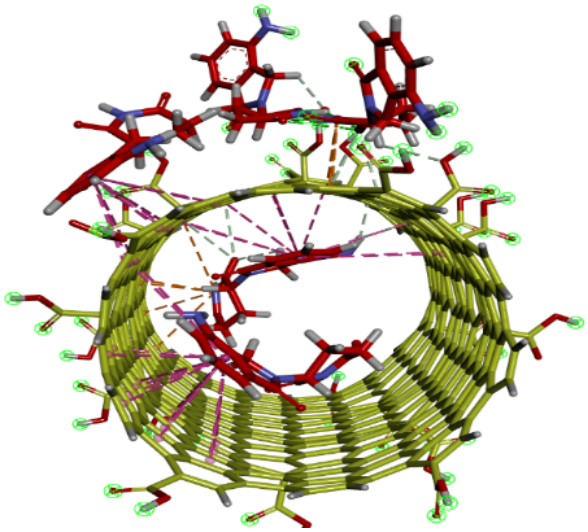

Figure 7. The interaction of drug molecules with different parts of f-CNT (10,10) at the end of simulation.

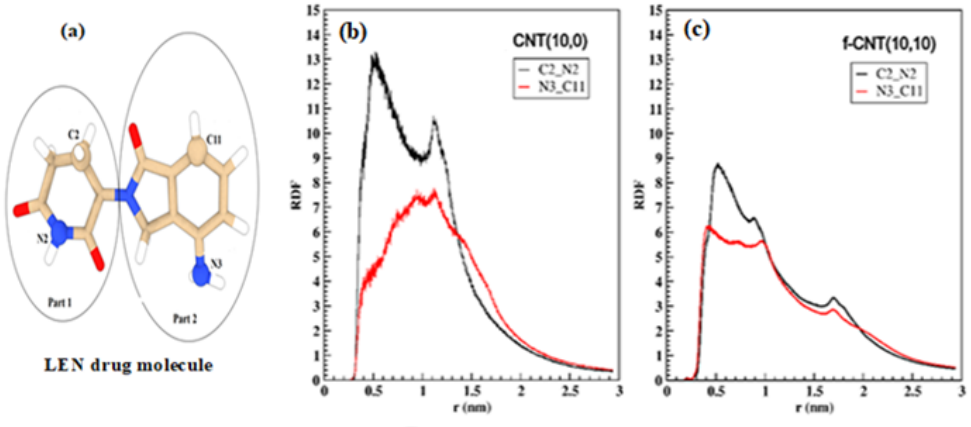

Figure 8. RDF of atomic representatives of different parts of (a) LEN molecule, (b) LEN molecules around CNT (10,0), (c) LEN molecules around f-CNT (10,10) in the simulation systems.

observed at 20 ns and 40 ns when all five drug molecules adsorbed on the f-CNT surface. On the other hand, the vdW interactions in the CNT (10,10) and f-CNT (10,10) systems were stronger compared to the other systems. It could be concluded that in the mentioned systems, the LEN molecules with stronger affinity interacted more favorably and formed more stable LEN/f-CNT, LEN/CNT complexes than f-CNT/CNT (10,0) and f-CNT/CNT (10,5) models. In this regard, the encapsulation of two drug molecules into f-CNT (10,10) led to a considerable decrease in vdW energy at 37 ns to the end of simulation and vdW energy value reached about −500 kJ/mol at the end of simulation (Figs. 9, 10, and Fig. 11).

3.5 The nAC and hydrogen interactions

Figs. 12 (a, b) showed that by starting the simulation and approaching drug molecules to the f-CNTs/CNTs surfaces, the nAC starts to increase. By adsorption of drugs on f-CNTs/CNTs surfaces, the nAC in all systems significantly increased. The curves showed that functionalization of CNTs increased considerably nAC between the LEN molecules and armchair and chiral nanotubes which indicated that carboxylic functional groups played a significant role in increasing the interactions between drug molecules and the mentioned nanotubes and as a result drug adsorption on them. The nAC between the LEN molecules and f-CNTs/CNTs was as a function of chirality. The trend of changes in the nAC between LEN molecules and f-CNTs/CNTs was similar and it followed the order of (10,10) > (10,5) > (10,0) at the corresponding simulation systems. But, their fluctuations were more intense in f-CNTs than CNTs. As the result presented in Figs. 12 (a, b), the maximum nAC for the LEN/CNTs systems belongs to the f-CNT and CNT with chirality (10,10) and at the end of simulation, the nAC for CNT (10,10) and f-CNT (10,10) were about 3000 (CNTs) and 5000 (f-CNTs), respectively. On the other hand, in the CNT/ f-CNT (10,0), the nAC were lower than other systems, and at 32 ns and 47 ns of simulation time, the number of them for f-CNT (10,0) was close to zero. In addition, the highest atomic contacts between drug molecules and f-CNT (10,0) were observed at 20 ns and 40 ns when all five drug molecules adsorbed on f-CNT surface (Fig. 10). There was an excellent correlation between the nAC and vdW energy values during the simulation time indicating that by increasing the nAC between drug molecules and nanotubes, vdW interactions between drug molecules and

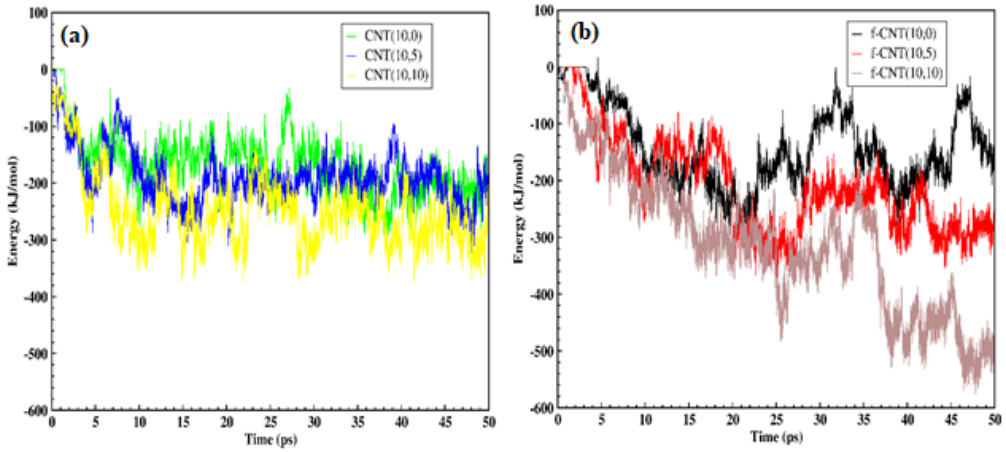

Figure 9. The energy values of vdW interactions (a) LEN molecules and, CNTs (b) LEN molecules and f-CNTs, with different chirality as a function of simulation time.

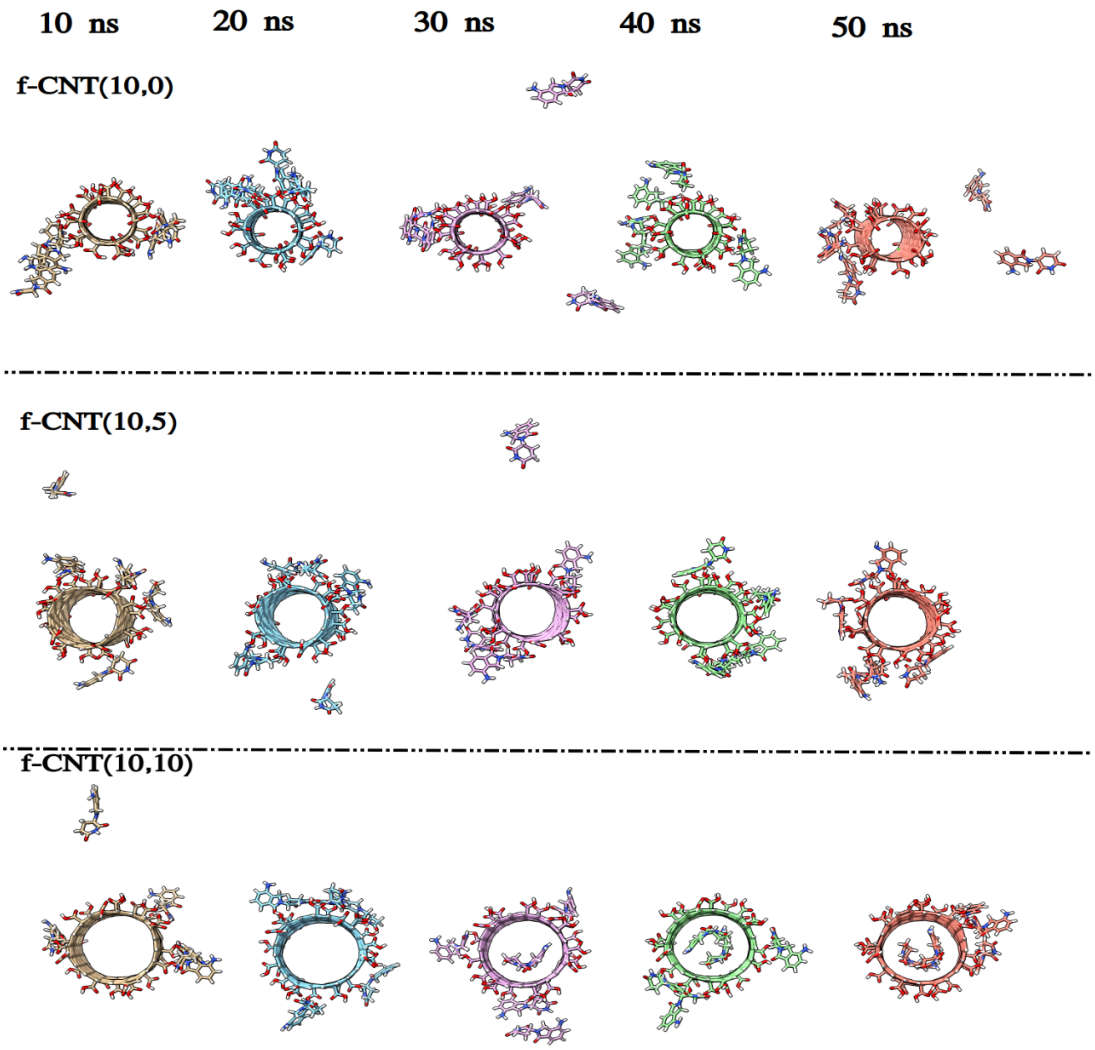

Figure 10. Schematic snapshots according to the interaction of LEN molecules with f-CNTs at five different times of simulation: 10 ns, 20 ns, 30 ns, 40 ns and 50 ns.

nanotubes were stronger and the vdW energy of these interactions decreased.

In this research, for more clarification of the functional groups and chirality effects on the drug adsorption, the nHBs between carboxylic functional groups of f-CNTs and LEN molecules were computed. Based on the results of theoretical and experimental research, HBs can improve the capacity of absorbance and enhance the drug stability [30]. Figs. 13 (a, b, c) represented that all f-CNTs formed HB bonds extensively with LEN molecules during simulation time. Maximum nHBs between LEN and chiral and zigzag f-CNTs were 5 and the maximum between armchair f-CNT and LEN were 4. But, armchair f-CNT formed HBs with LEN molecules earlier than other f-CNTs and after 1 ns from the starting simulation time. The results showed that from 30 ns to the end of the simulation time, the trend of changes in the nHBs between f-CNT (10,10) and drug molecules was a decreasing trend. The reason for this observation could be the encapsulation of two drug molecules inside the f-CNT (10,10) and their far away from the carboxylic functional groups. On the other hand, the trend of changes in the nHBs between f-CNT (10,5) and drug molecules from 30 ns to the end of the simulation time was an increasing trend. The reason for this observation could be the adsorption of all five drug molecules on the f-CNT (10,5) surface at the mentioned time range.

3.6 Solubility

Various factors, such as the nHBs formed between f-CNT and water molecules, SASA and ΔG_{sol} have been computed to investigate the effects of chirality and functional groups on the solubility of CNTs. The study revealed that in the examined systems, intermolecular HBs could potentially be established between heteroatoms present in f-CNTs and water molecules [49]. Figs. 14 (a, b) showed the intermolecular HBs formed between f-CNTs with different chiralities and water molecules. At the beginning of the simulation, the nHB interactions was about 66 interactions on average, and with the continuing the simulation, the number of interactions decreased and reached about 60 interactions in all three of the f-CNTs in around 20 ns. The possible reason for this reduction could be explained by the formation of HB interactions between the drug molecules and the f-CNTs, which has broken a nHBs between the water molecules and the f-CNTs. Furthermore, the graphs indicated that the

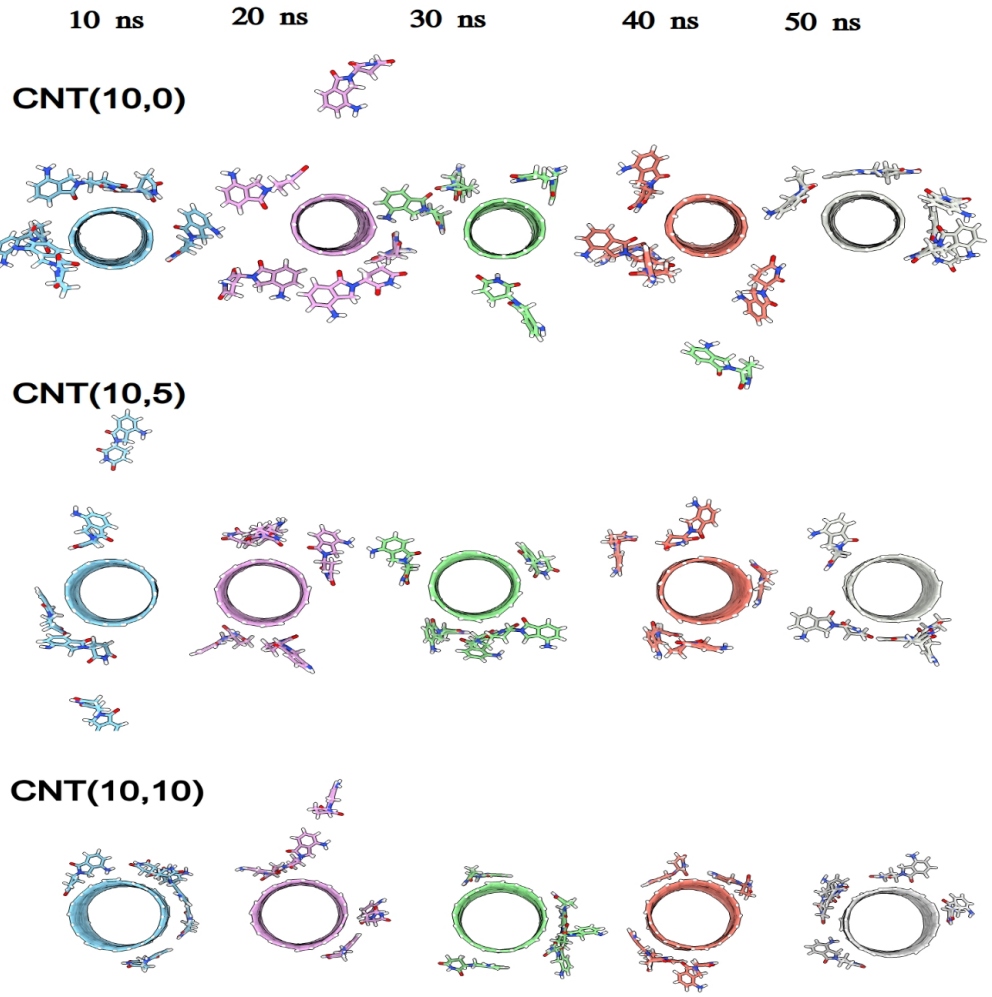

Figure 11. Schematic snapshots according to the interaction of LEN molecules with CNTs at five different times of simulation: 10 ns, 20 ns, 30 ns, 40 ns and 50 ns.

nHBs between the water molecules and the f-CNT (10,10) system were higher than the other f-CNTs. The graphs represented that from 25 ns to the end of the simulation time, the trend of changes in the nHBs between f-CNT (10,10) and water molecules was an increasing trend. The reason for this observation could be the encapsulation of two drug

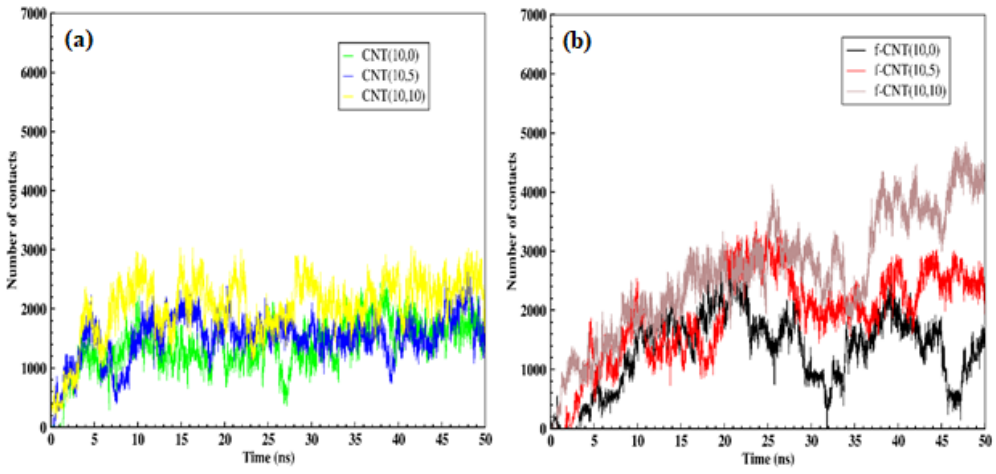

Figure 12. The nAC between (a) LEN molecules and CNTs and, (b) LEN molecules and f-CNTs, with different chiralities as a function of simulation time.

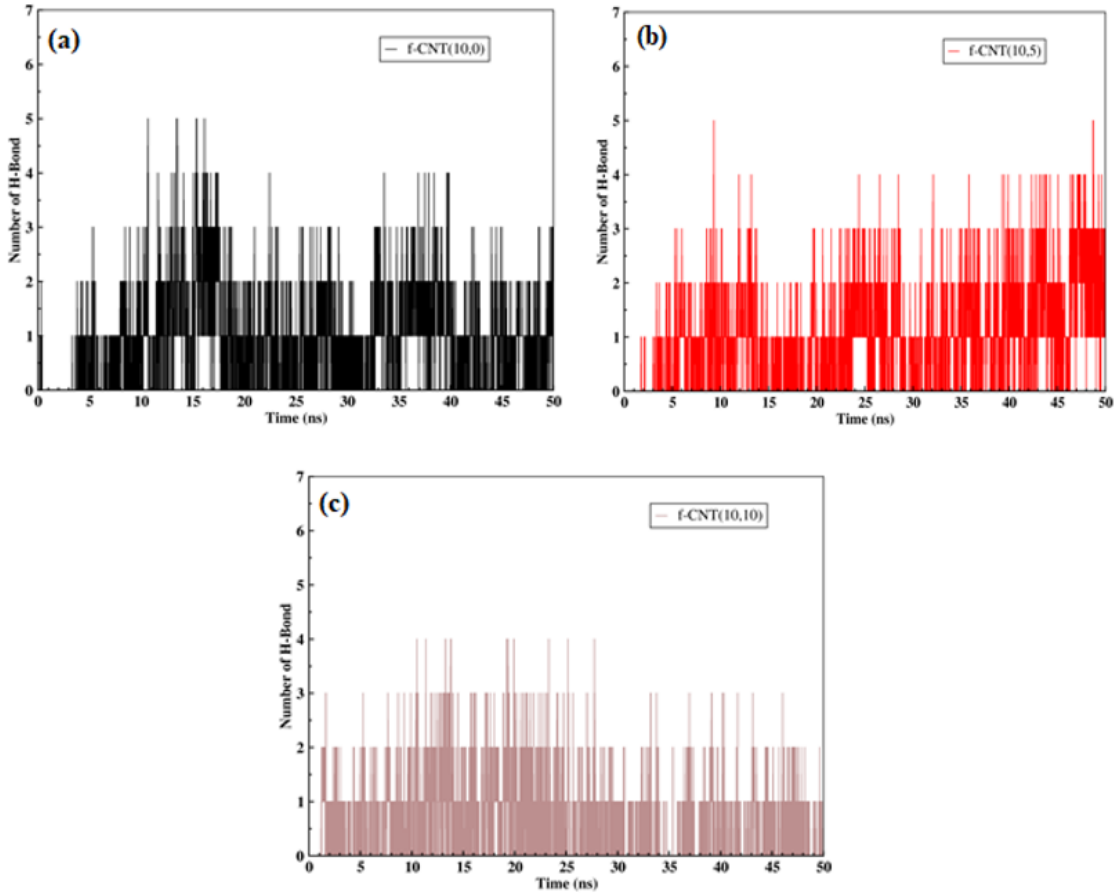

Figure 13. The nHBs between (a) LEN molecules and f-CNTs (10,0), (b) LEN molecules and f-CNTs (10,5), (c) LEN molecules and f-CNTs (10,10), with different chiralities as a function of simulation time.

molecules inside the f-CNT (10,10) and the availability of more carboxylic functional groups to form hydrogen bonds with water molecules. Therefore, armchair f-CNTs not only enhanced drug adsorption capacity but also had higher solubility in aqueous medium than other f-CNTs.

The SASA refers to the part of a compound's surface that can come into contact with solvent molecules. In Fig. 15 (a), the hydrophobic SASA was depicted for all simulation systems. The results showed that the functionalization of CNTs has increased SASA in all cases, and the lowest increase in SASA value was observed in CNT (10,0). The trend of SASA changes during the simulation time in f-CNTs and CNTs was similar and it followed the order of (10,10) > (10,5) > (10,0) at the corresponding simulation systems. The highest value of SASA (45 nm^2) for the f-CNT (10,10) compared to other CNTs confirmed that the armchair f-CNT

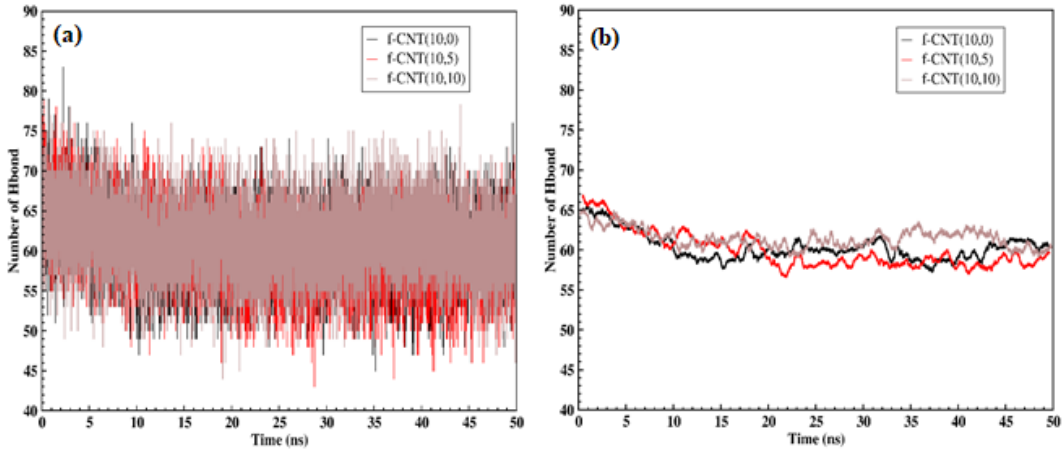

Figure 14. (a) The nHBs between water molecules and f-CNTs with different chiralities, (b) The average nHBs in f-CNTs with different chiralities during the simulation time.

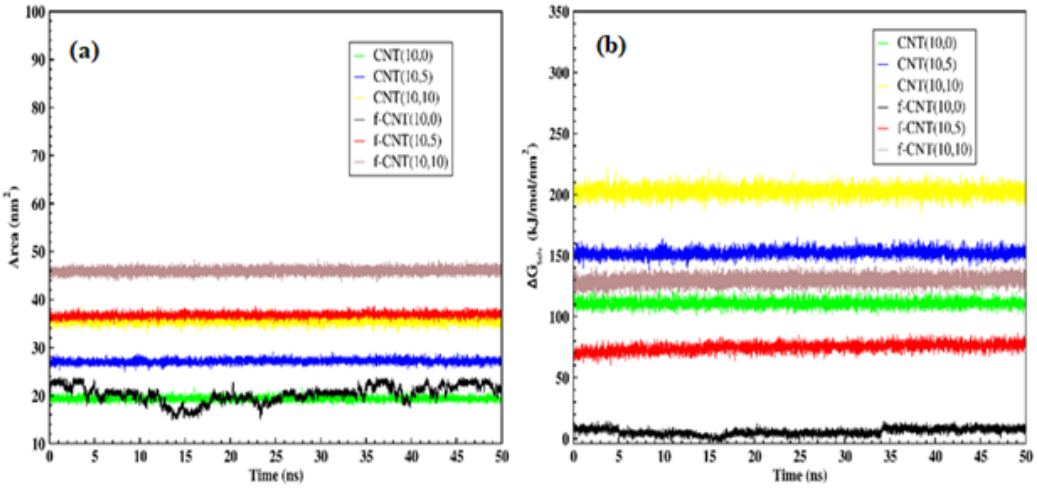

Figure 15. (a) SASA for CNTs and f-CNTs and, (b) ΔG_{sol} for CNTs and f-CNTs with different chiralities as a function of simulation time.

system provided more surface area available for interaction with water molecules.

One of the significant advances in theoretical chemistry was the accurate calculation of the solvation free energy (ΔG_{sol}) of molecules. ΔG_{sol} for f-CNTs/CNTs was computed and presented in Fig. 15 (b). The results showed that the functionalization of CNTs has decreased ΔG_{sol} in all cases, and the highest decrease in ΔG_{sol} value was observed in f-CNT (10,0). The trend of the ΔG_{sol} values in f-CNTs followed the order of (10,10) $>$ (10,5) $>$ (10,0) at the simulation systems which corresponds to the order of f-CNTs polarity. The findings from the nHBs, SASA and ΔG_{sol} showed that functionalization of CNTs increased their polarity and solubility. Moreover, these factors confirmed that the f-CNT (10,10) system exhibited the highest solubility among the investigated systems.

From the total results obtained in this study, it can be stated that the observed adsorption process between LEN and f-CNTs/CNTs was attributed to interactions such as $\pi - \pi$ stacking, hydrogen bonding, and van der Waals forces. Therefore, our results were in good agreement with the results reported in similar studies [28, 50].

4. Conclusion

MD simulations were used to investigate the adsorption mechanism of anticancer LEN drug in different positions on the surfaces of (zigzag (10,0), chiral (10,5) and armchair (10,10)) f-CNTs/CNTs with various chirality. RDFs, vdW energies, the nAC and nHBs between f-CNTs/CNTs and LEN/water molecules were studied to analyze effects of chirality and carboxylic functional groups. The results represented that the interaction strength of LEN/water molecules with both CNTs and f-CNTs was a function of chirality. The main interactions between LEN and f-CNT/CNT (10,0) were $\pi - \pi$ stacking and HBs interactions, while f-CNT/CNT (10,10) widely formed all three types of $\pi - \pi$ stacking, vdW and HBs interactions with LEN. Functionalization of CNTs with carboxylic functional groups also played a vital role in increasing vdW interactions and the stability of nanotubes, their polarity and solubility in water, and increasing nAC between the drug molecules and CNTs. In particular, functionalizing the CNT (10,10), in addition to increasing the drug adsorption capacity on this nanotube, also created the ability for drug molecules to spontaneously encapsulated inside nanotube during the simulation time. Encapsulation of two LEN molecules in f-CNT (10,10) increased the stability of the LEN-f-CNT complex by significantly reducing the vdW energy and increasing nAC between drug and the nanotube. In addition, this phenomenon increased the nHBs between f-CNT (10,10) and water molecules and increased the solubility of the nanotube.

Therefore, based on the simulation results in this work, we proposed f-CNT (10,10) as a suitable potential candidate for LEN delivery. In future studies, the role of drug-drug interactions during drug adsorption and encapsulation processes, as well as drug release from the surface and inside nanotubes, can be investigated using MD simulations and DFT methods.

Authors contributions
Authors have contributed equally in preparing and writing the manuscript.

Availability of data and materials
The authors declare that the data supporting the findings of this study are available within the paper.

Conflict of interests
The authors assert that they do not have any identifiable conflicting financial interests or personal relationships that might be perceived to influence the work presented in this paper.

References

[1] J. B. Bartlett, A. Michael, I. A. Clarke, K. Dredge, S. Nicholson, H. Kristeleit, A. Polychronis, H. Pandha, G. W. Muller, and D. I. Stirling. "Phase I study to determine the safety, tolerability and immunostimulatory activity of thalidomide analogue CC-5013 in patients with metastatic malignant melanoma and other advanced cancers.". *British Journal of Cancer*, 90:955–961, 2004. DOI: https://doi.org/10.1038/sj.bjc.6601579.

[2] X. Chen, D. Li, J. Wang, Z. Deng, and H. Zhang. "Lenalidomide acesulfamate: Crystal structure, solid state characterization and dissolution performance.". *Journal of Molecular Structure*, 1175:852–857, 2019.
DOI: https://doi.org/10.1016/j.molstruc.2018.08.059.

[3] C. Galustian and A. Dalgleish. "Lenalidomide: A novel anticancer drug with multiple modalities.". *Expert Opinion on Pharmacotherapy*, 10:125–133, 2009.
DOI: https://doi.org/10.1517/14656560802627903.

[4] H. Quach, D. Ritchie, A. K. Stewart, P. Neeson, S. Harrison, M. J. Smyth, and H. M. Prince. "Mechanism of action of immunomodulatory drugs (IMiDS) in multiple myeloma.". *Leukemia*, 24:22–32, 2010.
DOI: https://doi.org/10.1038/leu.2009.236.

[5] A. E. Adallahb, I. H. Eissa, A. B. M. Mehany, H. Sakr, A. Atwa, K. El-Adl, and M. A. El-Zahabi. "Immunomodulatory quinazoline-based thalidomide analogs: Design, synthesis, apoptosis and anticancer evaluations.". *Journal of Molecular Structure*, 1281:135164, 2023.
DOI: https://doi.org/10.1016/j.molstruc.2023.135164.

[6] V. Kotla, S. Goel, S. Nischal, C. Heuck, K. Vivek, B. Das, and A. Verma. "Mechanism of action of lenalidomide in hematological malignancies.". *Journal of Hematology & Oncology*, 2:1–10, 2009.
DOI: https://doi.org/10.1186/1756-8722-2-36.

[7] X. Armoiry, G. Aulagner, and T. Facon. "Lenalidomide in the treatment of multiple myeloma: A review.". *Journal of Clinical Pharmacy and Therapeutics*, 33:219–226, 2008.
DOI: https://doi.org/10.1111/j.1365-2710.2008.00920.x.

[8] Y. V. Meruvia-Rojas, E. Molina-Montes, A. Hernández-Laguna, and C. I. Sainz-Díaz. "Intercalation of the anticancer drug lenalidomide into montmorillonite for bioavailability improvement: A computational study.". *Journal of Molecular Modeling*, 31:5, 2024.
DOI: https://doi.org/10.1007/s00894-024-06210-w.

[9] A. Ghasemi Gol, J. Akbari, and M. Khalaj. "An Iron-enhanced nanocone assisted drug delivery of Aspirin: DFT assessments.". *International Journal of Nano Dimension*, 14:339–347, 2023.
DOI: https://doi.org/10.22034/ijnd.2023.1994253.2245.

[10] M. S. Sadjadi, B. Sadeghi, and K. Zare. "Natural bond orbital (NBO) population analysis of cyclic thionylphosphazenes, [NSOX (NPCl2)2]; X=F(1), X=Cl(2).". *Journal of Molecular Structure: THEOCHEM*, 817:27–33, 2007.
DOI: https://doi.org/10.1016/j.theochem.2007.04.015.

[11] K. Zare, N. Shadmani, and E. Pournamdari. "DFT/NBO study of Nanotube and Calixarene with anti-cancer drug.". *Journal of Nanostructure in Chemistry*, 3:1–6, 2013.
DOI: https://doi.org/10.1186/2193-8865-3-75.

[12] Z. Fei and M. Yoosefian. "Design and development of polymeric micelles as nanocarriers for anti-cancer Ribociclib drug.". *Journal of Molecular Liquids*, 329:115574, 2021.
DOI: https://doi.org/10.1016/j.molliq.2021.115574.

[13] B. Sadeghy and S. Ghammamy. "Oxidation of alcohols with tetramethylammonium fluorochromate in acetic acid.". *Russian Journal of General Chemistry*, 75:1886–1888, 2005.
DOI: https://doi.org/10.1007/s11176-006-0008-0.

[14] B. Sadeghi, S. Ghammamy, Z. Gholipour, M. Ghorchibeigy, and A. A. Nia. "Gold/hydroxypropyl cellulose hybrid nanocomposite constructed with more complete coverage of gold nano-shell.". *Micro & Nano Letters*, 6:209–213, 2011.
DOI: https://doi.org/10.1049/mnl.2011.0036.

[15] S. Esfahani, J. Akbari, and S. Soleimani-Amiri. "Adsorption of ibuprofen by an iron-doped silicon carbide graphene monolayer: DFT exploration of drug delivery insights.". *International Journal of Nano Dimension*, 15:63–71, 2024. URL https://creativecommons.org/licenses/by-nc/4.0.

[16] P. Hakemi, A. Ghadi, S. Mahjoub, E. Zabihi, and H. Tashakkorian. "Fabrication of PCL-PEG-PCL nanocarrier for Co-loading of Docetaxel/Quercetin and assessment of its effect on growth inhibition of human liver cancer (Hep-G2) cell line.". *International Journal of Nano Dimension*, 12:355–368, 2021. URL http://creativecommons.org/licenses/by/4.0.

[17] M. A. S. Sadjadi, M. Meskinfam, B. Sadeghi, H. Jazdarreh, and K. Zare. "In situ biomimetic synthesis and characterization of nano hydroxyapatite in gelatin matrix.". *Journal of Biomedical Nanotechnology*, 7:450–454, 2011.
DOI: https://doi.org/10.1166/jbn.2011.1305.

[18] A. Amininia, K. Pourshamsian, and B. Sadeghi. "Nano-ZnO impregnated on starch—A highly efficient heterogeneous bio-based catalyst for one-pot synthesis of pyranopyrimidinone and xanthene derivatives as potential antibacterial agents.". *Russian Journal of Organic Chemistry*, 56:1279–1288, 2020.
DOI: https://doi.org/10.1134/S1070428020070234.

[19] S. Ajori, S. Haghighi, and R. Ansari. "Buckling behavior of Carbon nanotubes functionalized with Carbene under physical adsorption of polymer chains: A molecular dynamics study.". *Brazilian Journal of Physics*, 47:606–616, 2017.
DOI: https://doi.org/10.1007/s13538-017-0528-6.

[20] S. Ajori, S. Haghighi, and R. Ansari. "Tensile characteristics of carbene-functionalized CNTs subjected to physisorption of polymer chains: A molecular dynamics study.". *Journal of Molecular Modeling*, 25:318, 2019.
DOI: https://doi.org/10.1007/s00894-019-4189-y.

[21] A. Esmaeili, M. Yoosefian, and M. Mahani. "Molecular Dynamics simulation of lenalidomide interaction with cRBN Protein: a target for immunomodulatory Drugs.". *South African Journal of Chemistry*, 77:157–162, 2023.
DOI: https://doi.org/10.17159/0379-4350/2023/v77a20.

[22] M. Rezazade, S. Ketabi, and M. Qomi. "Effect of functionalization on the adsorption performance of carbon nanotube as a drug delivery system for imatinib: molecular simulation study.". *BMC Chemistry*, 18:85, 2024.
DOI: https://doi.org/10.1186/s13065-024-01197-0.

[23] C. Arib and J. Spadavecchia. "Lenalidomide (LENA) hybrid gold complex nanoparticles: Synthesis, physicochemical evaluation, and perspectives in nanomedicine.". *ACS Omega*, 5:28483–28492, 2020.
DOI: https://doi.org/10.1021/acsomega.0c02644.

[24] S. A. Mallina and R. Sundararajan. "Lenalidomide loaded lactoferrin nanoparticle for controlled delivery and enhanced therapeutic efficacy.". *Research Journal of Pharmacy and Technology*, 11: 4010–4014, 2018.
DOI: https://doi.org/10.5958/0974-360X.2018.00737.0.

[25] S. Ajori, S. Haghighi, and R. Ansari. "A molecular dynamics study on the buckling behavior of cross-linked functionalized carbon nanotubes under physical adsorption of polymer chains.". *Applied Surface Science*, 427:704–714, 2018.
DOI: https://doi.org/10.1016/j.apsusc.2017.08.049.

[26] A. Moghaddam Jafari, A. Morsali, M. R. Bozorgmehr, S. A. Beyramabadi, and S. Mohseni. "Modeling and characterization of lenalidomide-loaded tripolyphosphate-crosslinked chitosan nanoparticles for anticancer drug delivery.". *International Journal of Biological Macromolecules*, 260:129360, 2024.
DOI: https://doi.org/10.1016/j.ijbiomac.2024.129360.

[27] H. Harati, A. Morsali, M. R. Bozorgmehr, and S. A. Beyramabadi. "β-cyclodextrin-lenalidomide anticancer drug delivery nanosystem: A quantum chemical approach.". *Journal of Molecular Liquids*, 344: 117762, 2021.
DOI: https://doi.org/10.1016/j.molliq.2021.117762.

[28] S. Sharifi, M. Sheikhi, S. Shahab, S. Kaviani, and R. Kumar. "DFT Study on the Interaction of Lenalidomide Anticancer Drug on the Surface of B12N12 Nanocluster.". *Letters in Organic Chemistry*, 19: 583–595, 2022.
DOI: https://doi.org/10.2174/1570178618666211027102305.

[29] H. S. Sayiner, F. Kandemirli, S. S. Dalgic, M. Monajjemi, and F. Mollaamin. "Carbazochrome carbon nanotube as drug delivery nanocarrier for anti-bleeding drug: Quantum chemical study.". *Journal of Molecular Modeling*, 28:11, 2022.
DOI: https://doi.org/10.1007/s00894-021-04948-1.

[30] A. Rezaei, A. Morsali, M. R. Bozorgmehr, and M. Nasrabadi. "Quantum chemical analysis of 5-aminolevulinic acid anticancer drug delivery systems: Carbon nanotube, –COOH functionalized carbon nanotube and iron oxide nanoparticle.". *Journal of Molecular Liquids*, 340:117182, 2021.
DOI: https://doi.org/10.1016/j.molliq.2021.117182.

[31] S. B. B. Ahamed, F. B. Ibrahim, and H. Srinivasan. "Cancer nanomedicine: A review on approaches and applications towards targeted drug delivery.". *International Journal of Nano Dimension*, 12:310–327, 2021. URL http://creativecommons.org/licenses/by/4.0.

[32] E. Rahmanifar, M. Yoosefian, and H. Karimi-Maleh. "Electronic properties and reactivity trend for defect functionalization of single-walled carbon nanotube with B, Al, Ga atoms.". *Synthetic Metals*, 221:242–246, 2016.
DOI: https://doi.org/10.1016/j.synthmet.2016.09.017.

[33] M. Zaboli, H. Raissi, and M. Zaboli. "Investigation of nanotubes as the smart carriers for targeted delivery of mercaptopurine anticancer drug.". *Journal of Biomolecular Structure and Dynamics*, 40: 4579–4592, 2022.
DOI: https://doi.org/10.1080/07391102.2020.1860823.

[34] H. Sun, P. She, G. Lu, K. Xu, W. Zhang, and Z. Liu. "Recent advances in the development of functionalized carbon nanotubes: A versatile vector for drug delivery.". *Journal of Materials Science*, 49: 6845–6854, 2014.
DOI: https://doi.org/10.1007/s10853-014-8436-4.

[35] H. Hashemzadeh and H. Raissi. "The functionalization of carbon nanotubes to enhance the efficacy of the anticancer drug paclitaxel: A molecular dynamics simulation study.". *Journal of Molecular Modeling*, 23:1–10, 2017.
DOI: https://doi.org/10.1007/s00894-017-3391-z.

[36] R. Narkhede, M. More, S. Patil, P. Patil, A. Patil, and P. Deshmukh. "Eco-friendly synthesis of surface grafted Carbon nanotubes from sugarcane cubes for the development of prolonged release drug delivery platform.". *International Journal of Nano Dimension*, 12: 211–221, 2021. URL http://creativecommons.org/licenses/by/4.0.

[37] M. Yoosefian and M. Jahani. "A molecular study on drug delivery system based on carbon nanotube for the novel norepinephrine prodrug, Droxidopa.". *Journal of Molecular Liquids*, 284:258–264, 2019.
DOI: https://doi.org/10.1016/j.molliq.2019.04.016.

[38] M. Kamel, H. Raissi, A. Morsali, and M. Shahabi. "Assessment of the adsorption mechanism of Flutamide anticancer drug on the functionalized single-walled carbon nanotube surface as a drug delivery vehicle: An alternative theoretical approach based on DFT and MD.". *Applied Surface Science*, 434:492–503, 2018.
DOI: https://doi.org/10.1016/j.apsusc.2017.10.165.

[39] S. Jo, T. Kim, V. G. Iyer, and W. Im. "CHARMM-GUI: a web-based graphical user interface for CHARMM.". *Journal of Computational Chemistry*, 29:1859–1865, 2008.
DOI: https://doi.org/10.1002/jcc.20945.

[40] M. J. Abraham, T. Murtola, R. Schulz, S. Páll, J. C. Smith, B. Hess, and E. Lindahl. "GROMACS: High performance molecular simulations through multi-level parallelism from laptops to supercomputers.". *SoftwareX*, 1-2:19–25, 2015.
DOI: https://doi.org/10.1016/j.softx.2015.06.001.

[41] J. Huang and A. D. MacKerell Jr. "CHARMM36 all-atom additive protein force field: Validation based on comparison to NMR data.". *Journal of Computational Chemistry*, 34:2135–2145, 2013.
DOI: https://doi.org/10.1002/jcc.23354.

[42] W. L. Jorgensen, J. Chandrasekhar, J. D. Madura, R. W. Impey, and M. L. Klein. "Comparison of simple potential functions for simulating liquid water.". *Journal of Chemical Physics*, 79:926–935, 1983.
DOI: https://doi.org/10.1063/1.445869.

[43] T. Darden, D. York, and L. Pedersen. "Particle mesh Ewald: An N·log(N) method for Ewald sums in large systems.". *Journal of Chemical Physics*, 98:10089–10092, 1993.
DOI: https://doi.org/10.1063/1.464397.

[44] M. Yousefi, M. Salehi Rad, R. Shakibazadeh, L. Ghodrati, and M. Ataie Kachoie. "Simulating a heteroatomic CBN fullerene-like nanocage towards the drug delivery of fluorouracil.". *Molecular Simulation*, 48:1284–1292, 2022.
DOI: https://doi.org/10.1080/08927022.2022.2086252.

[45] T. Chen, M. Li, and J. Liu. "π–π stacking interaction: A nondestructive and facile means in material engineering for bioapplications.". *Crystal Growth & Design*, 18:2765–2783, 2018.
DOI: https://doi.org/10.1021/acs.cgd.7b01503.

[46] R. Razavi and S. A. Ahmadi. "Molecular machine based on Rotaxane@Tricyclic antidepressant carrier: Theoretical molecular dynamic simulation.". *Computational and Theoretical Chemistry*, 1197: 113138, 2021.
DOI: https://doi.org/10.1016/j.comptc.2020.113138.

[47] A. Kordzadeh, S. Amjad-Iranagh, M. Zarif, and H. Modarress. "Adsorption and encapsulation of the drug doxorubicin on covalent functionalized carbon nanotubes: A scrutinized study by using molecular dynamics simulation and quantum mechanics calculation.". *Journal of Molecular Graphics and Modelling*, 88:11–22, 2019.
DOI: https://doi.org/10.1016/j.jmgm.2018.12.009.

[48] A. Kordzadeh, M. Zarif, and S. Amjad-Iranagh. "Molecular dynamics insight of interaction between the functionalized-carbon nanotube and cancerous cell membrane in doxorubicin delivery.". *Computer Methods and Programs in Biomedicine*, 230:107332, 2023.
DOI: https://doi.org/10.1016/j.cmpb.2022.107332.

[49] F. Najafi. "Thermodynamic studies of carbon nanotube interaction with Gemcitabine anticancer drug: DFT calculations.". *Journal of Nanostructure in Chemistry*, 10:227–242, 2020.
DOI: https://doi.org/10.1007/s40097-020-00344-y.

[50] A. Berisha. "Density functional theory and quantum mechanics studies of 2D carbon nanostructures (graphene and graphene oxide) for Lenalidomide anticancer drug delivery.". *Computational and Theoretical Chemistry*, 1230:114371, 2023.
DOI: https://doi.org/10.1016/j.comptc.2023.114371.